Homology groups of embedded fractional Brownian motion

H. Masoomy [1,*] S. Tajik,[2,†] and S. M. S. Movahed [1,‡]
[1]*Department of Physics, Shahid Beheshti University, 1983969411, Tehran, Iran*
[2]*Department of Physics, Brock University, St. Catharines, Ontario L2S 3A1, Canada*

(Received 16 June 2022; accepted 17 November 2022; published 12 December 2022)

A well-known class of nonstationary self-similar time series is the fractional Brownian motion (fBm) considered to model ubiquitous stochastic processes in nature. Due to noise and trends superimposed on data and even sample size and irregularity impacts, the well-known computational algorithm to compute the Hurst exponent (H) has encountered superior results. Motivated by this discrepancy, we examine the homology groups of high-dimensional point cloud data (PCD), a subset of the unit D-dimensional cube, constructed from synthetic fBm data as a pipeline to compute the H exponent. We compute topological measures for embedded PCD as a function of the associated Hurst exponent for different embedding dimensions, time delays, and amount of irregularity existing in the dataset in various scales. Our results show that for a regular synthetic fBm, the higher value of the embedding dimension leads to increasing the H dependency of topological measures based on zeroth and first homology groups. To achieve a reliable classification of fBm, we should consider the small value of time delay irrespective of the irregularity presented in the data. More interestingly, the value of the scale for which the PCD to be path connected and the postloopless regime scale are more robust concerning irregularity for distinguishing the fBm signal. Such robustness becomes less for the higher value of the embedding dimension. Finally, the associated Hurst exponents for our topological feature vector for the S&P500 were computed, and the results are consistent with the detrended fluctuation analysis method.

DOI: 10.1103/PhysRevE.106.064115

I. INTRODUCTION

Data generation from a wide range of experiments and observations leads to great opportunities to use modeling in the context of complex systems. Assigning a *shape* to various types of data and accordingly computing their persistence in terms of so-called resolution has recently become the focus of many studies. Furthermore, the spatiotemporal distribution (shape) of datasets has been beneficial in various branches of science [1–3]. Among different criteria such as linear algebra [4,5] and common statistical properties [6–13], the geometrical and topological features have provided complementary evaluations [14,15]. Depending on what type of information is needed and based on limitations in computational resources, one- and/or n-point statistics of geometrical and topological properties [16–24], and complex network-based analysis [9–13], and references therein], can be taken into account.

Inspired by geometrical fractals [25], the notion of self-similarity and self-affinity is employed to quantify the statistical properties of different fields of generally $(N + D)$ dimensions [14,26]. A pioneering method to quantify a self-similar process based on the Hurst exponent [27], which is known as fractional Brownian motion (fBm) [its associated increment is called fractional Gaussian noise (fGn)] [28], is called multifractal detrended fluctuation analysis (MFDFA) [29–31]. Besides the noted methods for classification, prediction, and examination of datasets, one can focus on topological features of data to study the data under the banner of topological data analysis (TDA) [34–38] and accordingly construct a powerful algebra-topological-based approach [39–41]. To this end, persistent homology (PH) as a shape-based tool that examines the evolution of global features of the data related to topological invariants is utilized [42–47].

There are many methods to construct higher dimensional sets from a $(1 + 1)$-dimensional series and then implement TDA. The visibility graph method [48], correlation network method [49], and time-delay embedding (TDE) method [50,51] have been used as the preprocessing part on the input data. The visibility graph and correlation network methods construct a complex network from the time series by considering the visibility condition between data points of underlying data and correlation between subtime series of the dataset, respectively, while the TDE method maps the time series into a D-dimensional point cloud data (PCD) by a time-delay parameter, τ. There are also some undirected methods for converting time series to the complex network, in which the reconstructed PCD (by the TDE method) is converted to the network. The recurrence network method [52–54] and k-nearest-neighbor (kNN) network method [55] are the examples. Briefly, in the recurrence network method, the connections are considered based on the proximity of the embedded data points (state vectors), while in the kNN method all state vectors (nodes) are connected with their k nearest neighbors.

Quantifying the scaling exponent of fBm and fGn has been done with various methods [29–33], but the spurious

*hoseingmasoomy@gmail.com
†samintjk@gmail.com
‡s.movahed@sbu.ac.ir

effect of complicated trends, the impact of nonstationarities, the finite-size effect, and irregularities have remained as the main challenges in the mentioned algorithms [33,56–59]. Subsequently, some efforts have been devoted to removing or at least tuning down the above discrepancies from different points of view ranging from network analysis [60–63], to reconstructed phase space of fBm series with the TDE method in terms of recurrence network analysis [64] by taking into account the false nearest-neighbors algorithm [65] and mutual information method [66], to the recurrence network of fBms [67], to performing TDA on the weighted natural visibility graph constructed from fGn series [68].

The main purpose of this work is exploring among the topological-based data analysis methods to introduce a robust algorithm in computing Hurst exponent. More precisely, we are going to figure out how the reconstructed phase space (embedded PCD) of the fBm time series changes by varying the Hurst exponent and the algorithmic parameters of the TDE method, i.e., the embedding dimension, and the time delay. Furthermore, the influence of irregularity adjusted by a parameter, q, the fraction of the number of missing data points, T_{missing}, in the time series to its total number of data points, T, as a measure for the amount of irregularity of underlying dataset will be examined in this work. More precisely, we utilize the PH method to get deep insight into how the state vectors constructed with the TDE method are distributed from a topological viewpoint. One of the advantages of this idea is that we can study the global properties of the phase space measured by the population of the homology groups of the weighted topological space (called weighted simplicial complex) mapped from the corresponding reconstructed phase space. More importantly, we can also capture the evolution of these topological invariants by varying the proximity parameter (threshold), ϵ, continuously. Subsequently, we examine the behavior of the topological measures computed from the dth persistent diagram, $\mathcal{D}_d$, and dth Betti number, β_d, as a function of the proximity parameter (called dth Betti curve) for $d = 0, 1$. We also aim to find the optimal choice for the parameters D and τ to distinguish the fBms of various H and also the results would be robust against the irregularity.

The advantages and novelties of our paper are as follows:

(1) We implement the PH method to quantify the Hurst exponent of a typical fBm series. To this end, we will introduce nine topological measures which are sensitive to H.

(2) We will show that almost all introduced criteria are robust against irregularity irrespective of the value of the Hurst exponent of the underlying fBm.

(3) The influences of the embedding dimension (D) and time delay (τ) capable of introducing a so-called feature vector to capture the reliable Hurst exponent will be examined.

Our results indicate that the computed topological measures of embedded fBm are sensitive to the value of the Hurst exponent. Generally, the statistics of dth homology classes have strong Hurst dependency. The evolution of d-dimensional topological holes (d-holes) occurs in low (high) scales for fBms with $H \gtrsim 0.5$ ($H \lesssim 0.5$). This H dependency grows by increasing the dimension of constructed PCD; i.e., for a good estimation for H one can deal with high-dimensional PCD. The situation is more noticeable when the time series contains some irregularity. For a signal with a high value of irregularity, the proposed measures become more D-dependent and the accuracy of estimating the Hurst exponent decays for high-dimensional PCD. In other words, the topological features extracted from low-dimensional PCDs have the minimum q dependency, i.e., the features of two-dimensional reconstructed phase space are more robust than the D-dimensional PCD for $D > 2$ in the presence of irregularity, suggesting the best value $D = 2$ for the estimation of the Hurst exponent of irregular fBms.

The rest of this paper is organized as follows: In the next section, our methodology and pipeline for analysis of the fBm signal are introduced. The numerical results of synthetic fBm time series, via reconstructed phase-space distribution of the state vectors from the topological viewpoint, are given in Sec. III. We implement our pipeline on the S&P500 financial time series to estimate the associated Hurst exponent in Sec. IV. A summary and concluding remarks will be presented in Sec. V.

II. METHODOLOGY AND OUR PIPELINE

For the sake of clarity, we will give a brief about the computational methods utilized in this paper to assess synthetic fractional Brownian motion (fBm) signal by paying attention to the mathematical preliminaries. More precisely, the PH of reconstructed phase space (embedded PCD) from fBm for different noticeable specifications and our pipeline is explained in this section.

A. Time-delay embedding

The reconstruction of phase space from a typical time series has been implemented to capture the evolution of the deterministic and chaotic dynamical systems and determine the correlations between associated quantities [51,69]. Time -delay embedding (TDE) is a mathematically well-defined method to map a time series into high-dimensional Euclidean space to make such a finite-dimensional phase space [50]. For a given discrete time series, $x = \{x_t\}_{t=1}^{T}$, of length T, we make a set of N state vectors of dimension D in D-dimensional Euclidean space, $\mathbb{R}^D$, which is called D-dimensional PCD, for a given time delay, τ, as follows:

$$X(x, D, \tau) = \{\vec{x}_t \in \mathbb{R}^D \mid \vec{x}_t \equiv (x_t, x_{t+\tau}, \ldots, x_{t+(D-1)\tau})\}_{t=1}^{N}. \tag{1}$$

Notice that $X(x, D = 1, \tau) = x$ and the PCD size $N = T - (D - 1)\tau$. According to the Takens theorem [50], we can recreate a topologically equivalent D-dimensional phase space from a time series by means of this method. Figure 1 shows a synthetic fBm time series with $H = 0.5$ of length $T = 10^4$ (top panel) and associated two-dimensional PCD of size $N = 9 \times 10^3$ reconstructed by the TDE method for $\tau = 10^3$ (bottom panel). As noticed before, for any value of D and τ, one can construct PCD from fBm, $x(H, q, T)$, and therefore, the associated homology groups are examined.

B. Persistent homology

Topology is a branch of pure mathematics dealing with abstract objects living in high-dimensional topological spaces (e.g., the real line, sphere, torus, and more complicated

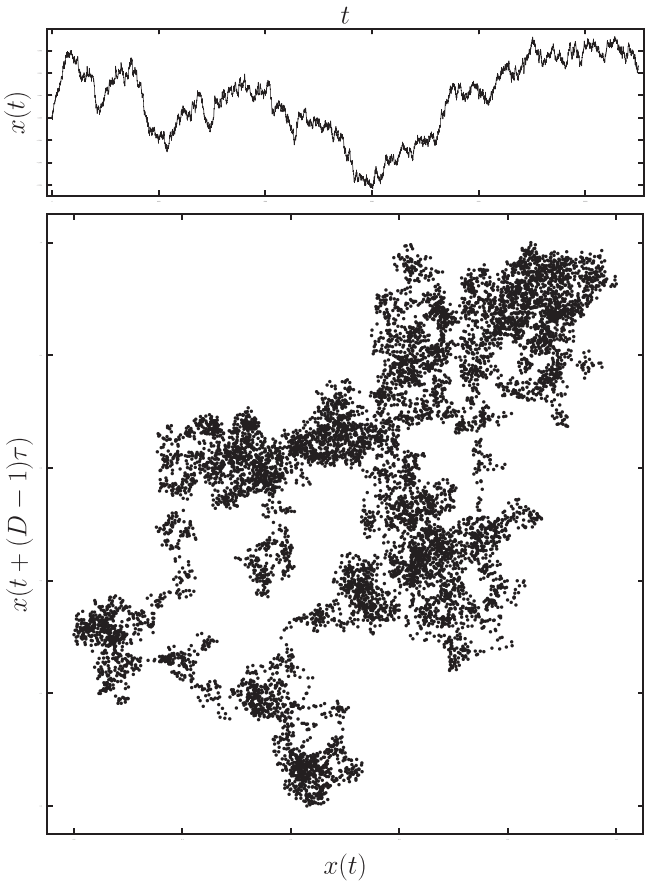

FIG. 1. A synthetic regular ($q = 0$) fBm time series of length $T = 10^4$ with $H = 0.5$ (top panel) and associated phase space of size $N = 9 \times 10^3$ reconstructed with the TDE method for embedding dimension $D = 2$ and time delay $\tau = 10^3$ (bottom panel).

spaces) to classify them in terms of their global properties (e.g., connectedness, genus, Euler characteristics, etc.) [39]. These global features of the space usually are topologically invariant, which means that they do not change under continuous deformations and are not dependent on the way the corresponding space is made (triangulated, mathematically). By the term continuous deformation, we mean any continuous changes (elastic motions) of the space like shrinking, stretching, rotating, reflecting, etc., but not cutting or gloving. These continuous deformations are defined by the concept of *homeomorphism* in algebraic topology [70].

Here we introduce the required objects and definitions in homology theory. In algebraic topology, to determine the topological properties of a space, the associated space is triangulated by mapping it into a collection of d-dimensional simplicies (d-simplicies), called a simplicial complex. A d-simplex $\sigma_d = [\vec{x}_0, \ldots, \vec{x}_d]$ is a convex-hull subset of d-dimensional Euclidean space, $\mathbb{R}^d$, determined by its $(d + 1)$ geometrically independent points $\{\vec{x}_0, \ldots, \vec{x}_d\}$ in $\mathbb{R}^d$. For instance, a point is a 0-simplex, a line segment is a 1-simplex, a triangle is a 2-simplex, a tetrahedron is a 3-simplex, etc. (see the left panel of Fig. 2). A simplicial complex, $\mathcal{K}$, is a collection of simplices such that any subsimplex of any simplex in the simplicial complex is in the simplicial complex. Also, any pair of simplices are either disjoint or they intersect in a lower-

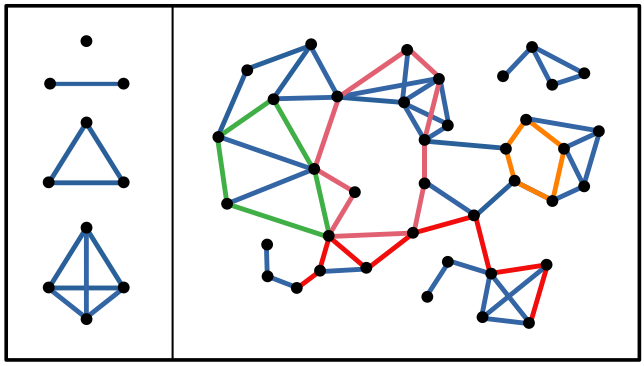

FIG. 2. Left panel: Low-dimensional simplicies, 0-simplex, 1-simplex, 2-simplex, and 3-simplex (sorted from top to bottom). Right panel: A three-dimensional simplicial complex containing $|\Sigma_0| = 39$ 0-simplicies, $|\Sigma_1| = 63$ 1-simplicies, $|\Sigma_2| = 25$ 2-simplicies, $|\Sigma_3| = 3$ 3-simplicies and determined by the Betti numbers $\vec{\beta} = (2, 4, 0, 0)$. The subspaces determined by different colors illustrate examples for a 1-chain (red), 1-cycle (pink), 1-boundary (green), and 1-hole (orange).

dimensional simplex existing in the simplicial complex. The dimension of a simplicial complex is defined as the dimension of the largest simplex in it (see the right panel of Fig. 2) [39]. For a simplicial complex, $\mathcal{K}$, containing $|\Sigma_d|$ d-simplices, one can create a $|\Sigma_d|$-dimensional vector space, $\mathcal{C}_d(\mathcal{K})$, called a d-chain group of the simplicial complex $\mathcal{K}$, by the basis considered as the set of all d-simplicies $\Sigma_d(\mathcal{K}) = \{\sigma_d^i\}_{i=1}^{|\Sigma_d|}$ of the $\mathcal{K}$ and the vectors, called d-chains, as follows:

$$c_d \equiv \sum_{i=1}^{|\Sigma_d|} a_i \sigma_d^i \,;\; a_i \in \mathbb{Z}_2 \equiv \{0, 1\}. \tag{2}$$

The boundary of a d-simplex is the union of all its $(d - 1)$-subsimplices, which is obtained by applying the boundary operator ∂_d on the simplex:

$$\partial_d(\sigma_d) = \sum_{i=0}^{d} (-1)^i \, [\vec{x}_0, \ldots, \vec{x}_{i-1}, \vec{x}_{i+1}, \ldots, \vec{x}_d]. \tag{3}$$

The d-cycle group $\mathcal{Z}_d(\mathcal{K}) \equiv \{c_d \in \mathcal{C}_d(\mathcal{K}) \mid \partial_d(c_d) = \emptyset\}$ of $\mathcal{K}$ is defined as the set of all boundaryless d-chains of the $\mathcal{K}$; i.e., any d-chain mapped to the empty space (set) is a d-cycle $z_d \in \mathcal{Z}_d(\mathcal{K})$. Another subspace of $\mathcal{C}_d(\mathcal{K})$ is called a d-boundary group $\mathcal{B}_d(\mathcal{K}) \equiv \{c_d \in \mathcal{C}_d(\mathcal{K}) \mid \partial_{d+1}(c_{d+1}) = c_d\}$ containing all d-chains of $\mathcal{K}$, which is the boundary of a $(d + 1)$-chain in $\mathcal{C}_{d+1}(\mathcal{K})$. The elements of $\mathcal{B}_d(\mathcal{K})$ are called a d-boundary. Since the boundary operator satisfies the property $\partial_{d-1}(\partial_d(c_d)) = \emptyset$ for any $c_d \in \mathcal{C}_d(\mathcal{K})$, we can conclude that $\mathcal{B}_d(\mathcal{K}) \subseteq \mathcal{Z}_d(\mathcal{K})$. In order to ignore d-cycles of the simplicial complex $\mathcal{K}$ that are also a boundary, one can consider a topological equivalence relation on $\mathcal{Z}_d(\mathcal{K})$ such that any pair of cycles $z_d^i, z_d^j \in \mathcal{Z}_d(\mathcal{K})$ are equivalent (homologous) if $z_d^i - z_d^j \in \mathcal{B}_d(\mathcal{K})$. This equivalence relation partitions $\mathcal{Z}_d(\mathcal{K})$ into a union of disjoint subsets, called dth homology classes. The d-homology group of the simplicial complex $\mathcal{K}$ is defined as $\mathcal{H}_d(\mathcal{K}) \equiv \{[z_d] \mid z_d \in \mathcal{Z}_d(\mathcal{K})\}$, where $[z_d]$ represents the homology class of z_d. The dth Betti number of simplicial complex $\mathcal{K}$, denoted by $\beta_d(\mathcal{K})$, as a topological invariant of

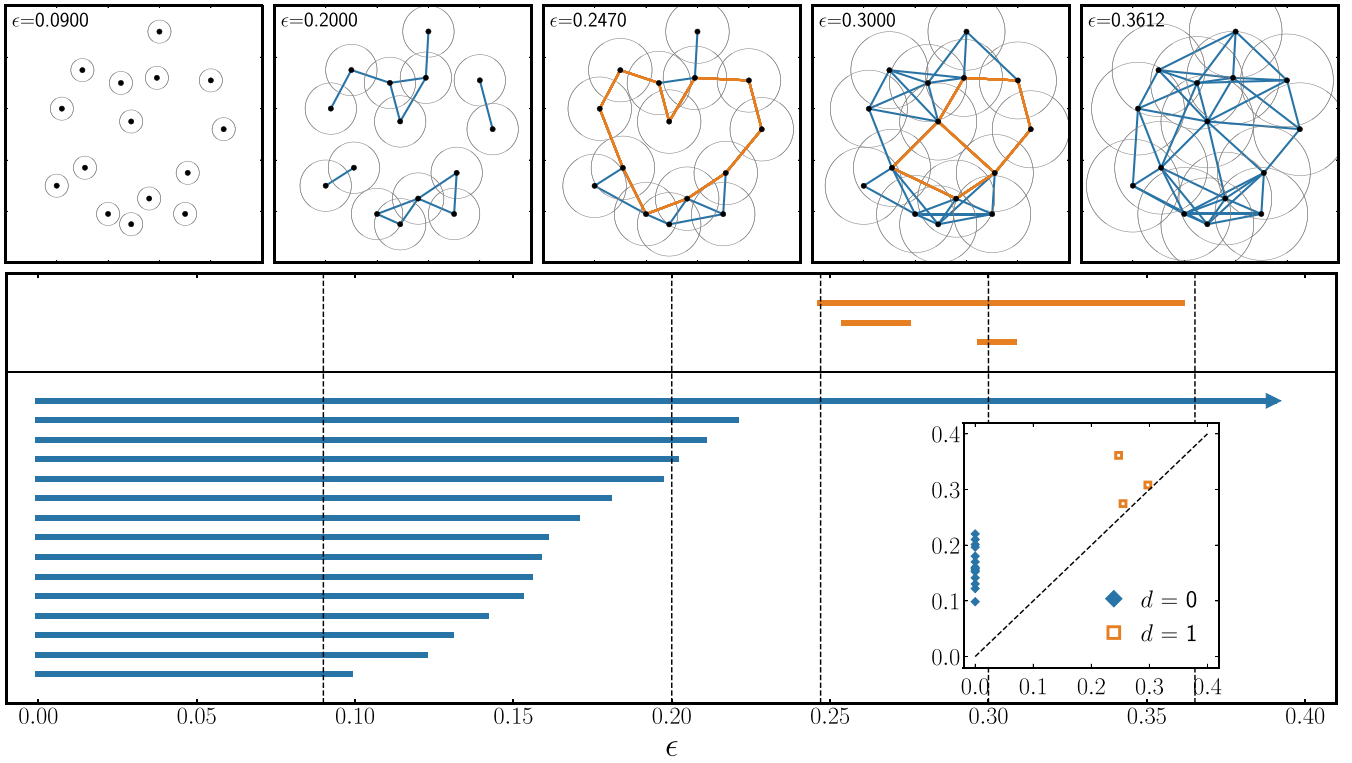

FIG. 3. The persistent homology (PH) of a random PCD. This figure shows how the PH method extracts the topological features of a random two-dimensional PCD of size $N = 15$. Top panel: Growing the VR simplicial complex by increasing the proximity parameter ϵ (from left to right). Through the filtration, topological properties of the PCD change (connected components represented by black points and blue lines, and topological loops represented by orange lines). Bottom panel: The PB (PD in inset) associated with the filtration shows the persistence (evolution) of extracted topological features by persistence bars (pairs); filled blue diamond and empty orange square symbols are for the zeroth and first homology generators, respectively.

$\mathcal{K}$, is the dimension of d-homology group of $\mathcal{K}$. Intuitively, $\beta_d(\mathcal{K})$ indicates the number of d-dimensional topological holes (d-holes) of the topological space triangulated by the simplicial complex $\mathcal{K}$.

Consider a D-dimensional PCD $X = \{\vec{x}_i \in \mathbb{R}^D \mid \vec{x}_i \equiv (x_i^\delta)_{\delta=1}^D\}_{i=1}^N$ of size N as a finite ($N \neq \infty$) discrete subset of D-dimensional Euclidean space $\mathbb{R}^D$. The first step to study this type of dataset from topological viewpoint, i.e., to understand the topological space underlying the PCD, is finding a triangulation to tessellate the dataset [35]. We construct a simplicial complex $\mathcal{K}$ from the PCD X. The obvious triangulation of X is creating a simplicial complex containing only N 0-simplices, $\mathcal{K}(X) = \{\sigma_0^i \equiv [\vec{x}_i] \mid \vec{x}_i \in X\}_{i=1}^N$, with trivial topology ($\beta_0[\mathcal{K}(X)] = N, \beta_d[\mathcal{K}(X)] = 0$ for $d > 0$). To go beyond this simple structure, one can build the simplicial complex of the PCD in larger scale, i.e., a higher value of proximity of the vectors in X. To this end, for a fixed value of the proximity parameter $\epsilon \geqslant 0$, we can create a simplicial complex $\mathcal{K}(X, \epsilon)$ associated with the PCD X, as a collection of simplcies such that any d-simplex $\sigma_d = [\vec{x}_0, \ldots, \vec{x}_d]$ in $\mathcal{K}(X, \epsilon)$ corresponds to $(d + 1)$ vectors $\{\vec{x}_0, \ldots, \vec{x}_d\}$ in X and the Euclidean distance between any pair of the vectors $\{\vec{x}_0, \ldots, \vec{x}_d\}$ is less than the threshold. The constructed simplicial complex $\mathcal{K}(X, \epsilon)$ is called a Vietoris-Rips (VR) simplicial complex [36]. After building the VR simplicial complex $\mathcal{K}(X, \epsilon)$ from the dataset, one can calculate the topological objects defined before. But the structural properties of $\mathcal{K}(X, \epsilon)$ are highly dependent on the chosen scale ϵ. To overcome this issue, the persistent homology (PH) method, from topological data analysis (TDA), computes the evolution of the extracted topological invariants (dth Betti numbers) by varying the proximity parameter ϵ continuously [71]. To be precise, PH builds a growing sequence of VR simplicial complexes, called filtration, by increasing the proximity parameter and captures the structural changes of the simplicial complex in terms of Betti numbers $\beta_d(\epsilon)$, called a Betti curve. Therefore, one can get the evolution of any dth homology class $[z_d]$ in a filtered simplicial complex expressed by persistence pair (PP) $\epsilon^{[z_d]} = (\epsilon^{[z_d]}_{\text{appear}}, \epsilon^{[z_d]}_{\text{disappear}})$ and summarize all PPs in a multiset $\mathcal{D}_d = \{\epsilon_i^{[z_d]}\}_i$, known as the dth persistence diagram (PD), where $\epsilon^{[z_d]}_{\text{appear}}$ and $\epsilon^{[z_d]}_{\text{disappear}}$ are the scales in which the homology class $[z_d]$ appears and disappears, respectively. Figure 3 illustrates the mechanism of homology class extraction from a typical random two-dimensional PCD of size $N = 15$ with the PH method. The top row shows the filtration process in which by increasing the proximity parameter (diameter of the gray circles centered by the state vectors) the topology of the VR simplicial complex varies. The zeroth (first) homology classes are represented by black points and blue lines (orange lines). The bottom panel indicates the persistence barcode (PB) and persistence diagram (PD) (inset plot) of the zeroth (blue bars in PB and filled blue points in PD) and first (orange bars in PB and orange empty points in PD) homology classes associated with the filtration.

FIG. 4. The proposed pipeline in this paper: A synthetic fractional Brownian motion (fBm) time series is converted to a point cloud data (PCD) with the time-delay embedding (TDE) method. The evolution of homology groups of a simplicial complex mapped from the constructed point cloud data with the Vitoris-Rips (VR) method is calculated with the persistent homology (PH) technique and summarized as persistence pairs (PPs) in persistence diagrams (PDs). Finally, topological measures based on the persistence diagrams and Betti curves are computed.

The number of PPs in the dth PD is called $n_d = |\mathcal{D}_d|$, and for $d = 0$, this quantity has trivial value $n_0 = N$. The reason is the correspondence between the state vectors and PPs in the zeroth PD. To quantify the distribution of PPs in the dth PD, one can calculate the Shannon entropy of the lifespans of the dth homology classes in $\mathcal{D}_d$. By the lifespan of a dth homology class $[z_d]$, we mean the positive quantity $\ell^{[z_d]} \equiv \epsilon^{[z_d]}_{\text{disappear}} - \epsilon^{[z_d]}_{\text{appear}}$. This measure for the entropy, so-called persistence entropy (PE), is formulated as follows:

$$E_d = -\sum_{i=1}^{n_d} \frac{\ell_i^{[z_d]}}{\sum_{i=1}^{n_d} \ell_i^{[z_d]}} \log\left(\frac{\ell_i^{[z_d]}}{\sum_{i=1}^{n_d} \ell_i^{[z_d]}}\right). \tag{4}$$

Betti curves are a common visualization of PDs which indicate how the population of homology classes (Betti numbers) evolve through the scale, ϵ. In fact, the number of d-holes of a filtered simplicial complex for a fixed value of ϵ, denoted by $\beta_d(\epsilon)$, is the number of PPs in dth PD for which $\epsilon^{[z_d]}_{(i)\text{appear}} \leqslant \epsilon$ and $\epsilon^{[z_d]}_{(i)\text{disappear}} > \epsilon$, $i = 1, \ldots, n_d$. Therefore, the calculation of the dth Betti curve can be written as

$$\beta_d(\epsilon) = \sum_{i=1}^{n_d} \Theta\big(\epsilon - \epsilon^{[z_d]}_{(i)\text{appear}}\big)\, \Theta\big(\epsilon^{[z_d]}_{(i)\text{disappear}} - \epsilon\big). \tag{5}$$

It is possible to define other relevant measures based on the behavior of Betti curves, e.g., $\epsilon_d^{\text{appear}}$, $\epsilon_d^{\text{diappear}}$, and $\epsilon_d^{\text{maximize}}$,

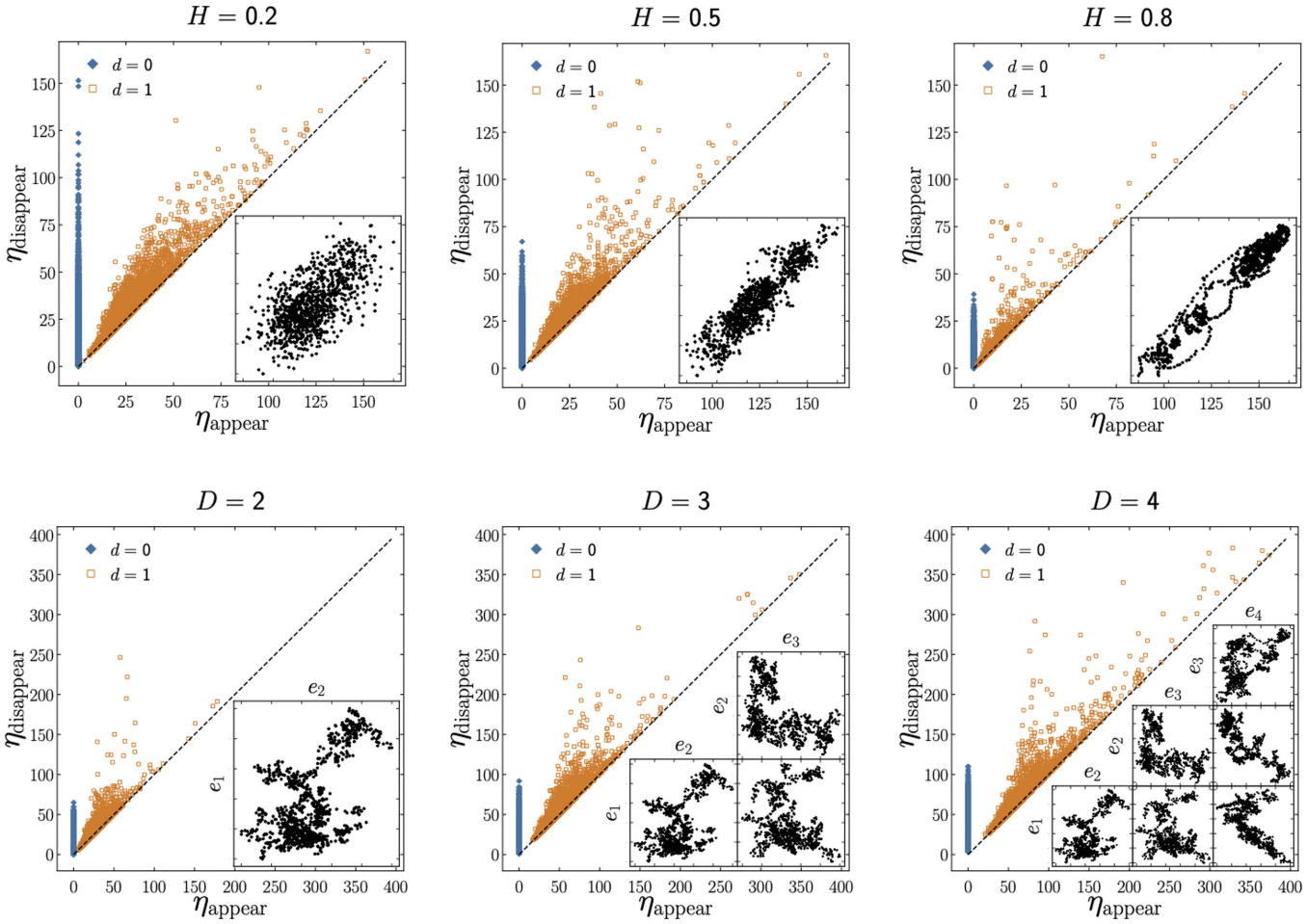

FIG. 5. Upper panels: The PDs of dth homology groups (filled blue diamond for $d = 0$ and empty orange square for $d = 1$) for two-dimensional PCD (inset plots) converted from regular fBm series with $H = 0.2$ (left), $H = 0.5$ (middle), and $H = 0.8$ (right) with the TDE method for time delay $\tau = 100$. The population and distribution of PPs varies by H, which cause the H dependency of topological measures. Lower panels: The D dependency of zeroth (filled blue diamond) and first (empty orange square) PD of regular fBm with $H = 0.5$ embedded to unit D cube ($D = 2, 3, 4$ from left to right) for $\tau = 1000$. The inset plots show the visualization of the reconstructed PCD projected to the standard planes of the space.

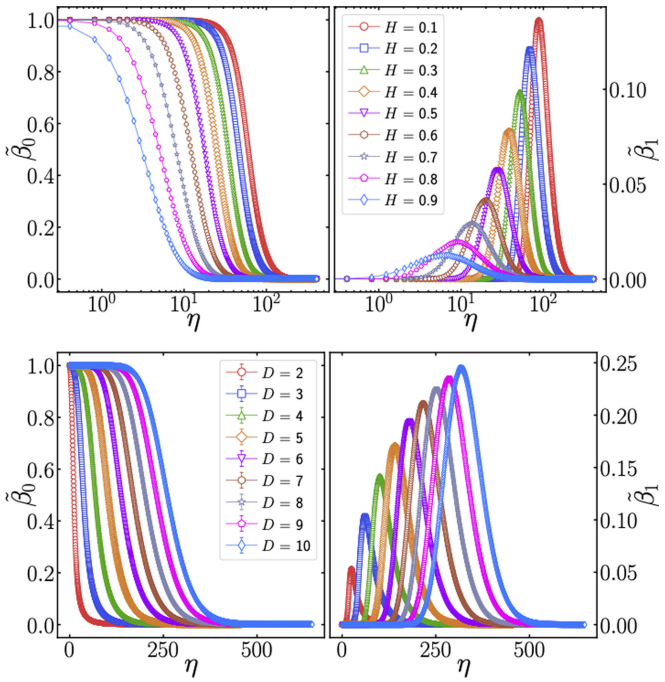

FIG. 6. Upper panels: The zeroth (left) and first (right) Betti curve of reconstructed four-dimensional phase space for time delay $\tau = 1$ from regular fBms of various Hurst exponents. Lower panels: The Betti curves of reconstructed phase space of various dimensions for time delay $\tau = 10$ from regular fBm series with $H = 0.1$. These curves indicate the strong D dependency of topological properties of the embedded PCD.

which are known as critical scales for the dth Betti curve, and they read as

$$\epsilon_d^{\text{appear}} \equiv \max\left(\epsilon \;\middle|\; \int_0^{\epsilon} \beta_d(\epsilon')\, d\epsilon' = 0\right) \tag{6}$$

and

$$\epsilon_d^{\text{diappear}} \equiv \min\left(\epsilon \;\middle|\; \int_{\epsilon}^{+\infty} [\beta_d(\epsilon') - c_d]\, d\epsilon' = 0\right), \tag{7}$$

where $c_{d=0} = 1$ and $c_{d>0} = 0$, and

$$\epsilon_d^{\text{maximize}} \equiv \min\left(\epsilon \;\middle|\; \frac{\partial \beta_d(\epsilon')}{\partial \epsilon'}|_{\epsilon'=\epsilon} = 0,\ \frac{\partial^2 \beta_d(\epsilon')}{\partial \epsilon'^2}|_{\epsilon'=\epsilon} \leqslant 0\right). \tag{8}$$

According to the structure of the VR simplicial complex at $\epsilon = 0$, we obtain $\epsilon_0^{\text{appear}} = \epsilon_0^{\text{maximize}} = 0$. Furthermore, for $d = 0$ the critical scale $\epsilon_0^{\text{disappear}}$ separates the connected regime ($\epsilon \geqslant \epsilon_0^{\text{disappear}}$) from the disconnected regime ($\epsilon < \epsilon_0^{\text{disappear}}$). For $d = 1$, the critical scales $\epsilon_1^{\text{appear}}$ and $\epsilon_1^{\text{disappear}}$ determine the loopless regimes (preloopless regime $\epsilon < \epsilon_1^{\text{appear}}$ and postloopless regime $\epsilon > \epsilon_1^{\text{disappear}}$) and $\epsilon_1^{\text{maximize}}$ is the scale at which the simplicial complex becomes loopful. The integration of the Betti curves is the last proposed measure:

$$B_d \equiv \int_{\epsilon_d^{\text{appear}}}^{\epsilon_d^{\text{disappear}}} \beta_d(\epsilon')\, d\epsilon'. \tag{9}$$

Now we are interested in analyzing the effect of the parameters D, τ, and q on the statistics of the dth homology group ($d = 0, 1$) and the H dependency of the mentioned nontrivial topological measures, namely, $\epsilon_0^{\text{disappear}}$, B_0, E_0, $\epsilon_1^{\text{appear}}$, $\epsilon_1^{\text{disappear}}$, $\epsilon_1^{\text{maximize}}$, B_1, E_1, and n_1 and to look for which ones are more appropriate for estimating the Hurst exponent of the fBm series in the presence of irregularity in detail in the next section.

C. Pipeline

Our proposed pipeline includes the following steps (see Fig. 4):

(1) The fBm series $x(H, q, T)$ of the distinct Hurst exponent H with some irregularity q with size T is simulated and embedded to a high-dimensional Euclidean space with the TDE method for embedding dimension D and time delay τ to construct a phase space $X(H, q, N, D, \tau)$ of size $N = T - (D-1)\tau$.

(2) The reconstructed phase space is mapped to the simplicial complex $\mathcal{K}(H, q, N, D, \tau, \epsilon)$ with the Vietoris-Rips (VR) method for various scales ϵ.

(3) The PH method is applied to extract the statistics and evolution of d-dimensional topological holes (d-holes) of the scale-dependent VR simplicial complex, and then the associated generators are visualized as PPs in the dth PD $\mathcal{D}_d(H, q, N, D, \tau)$ for zeroth and first homology groups.

(4) Some topological measures are directly computed from the PDs, and some others can be defined by the criticality of the behavior of the dth Betti curve $\beta_d(H, q, N, D, \tau, \epsilon)$ calculated from PDs.

It is worth noticing that we define the normalized quantities $\tilde{\beta}_d \equiv \beta_d/N$ and $\eta \equiv N\epsilon$ and use them to calculate the introduced topological measurements instead of the quantities β_d and ϵ in the rest of this paper.

III. RESULTS

According to our pipeline, first, we generate a synthetic fBm for any given Hurst exponent based on the Holmgren-Riemann-Liouville fractional integral [28,72,73]

$$x(H, t) = \frac{1}{\Gamma\left(H + \frac{1}{2}\right)} \int_0^t (t - s)^{H - \frac{1}{2}}\, dx(s), \tag{10}$$

where Γ is the Gamma function and $dx(s) = x(s + ds) - x(s)$ is the increment of $(1 + 1)$-dimensional Brownian motion (see [68] for more details). Then we convert and rescale our mock fBm time series of various Hurst exponent $H \in (0, 1)$ with $\Delta H = 0.1$ to the unit D-dimensional cube (D-cube) $[0, 1]^D$, a subspace of D-dimensional Euclidean space, from $D = 2$ to $D = 10$ ($\Delta D = 1$), by using the TDE method for $\tau = 1, 10, 100, 1000$ and irregularity value, defined as the fraction of missing data points in the time series to the time-series length $q \equiv T_{\text{missing}}/T$, from $q = 0$ (regular) to $q = 0.09$ by step $\Delta q = 0.01$. Notice that we have valued the length of time series T, such that the PCD size $N = T - (D-1)\tau$ is fixed $N = 2^{10}$ and the missing data points are selected uniformly randomly. In the PH part, the proximity parameter varies continuously from $\epsilon_{\min} = 0$ to $\epsilon_{\max} = 0.2\sqrt{D}$, where $\sqrt{D}$ is the maximum possible distance between any two

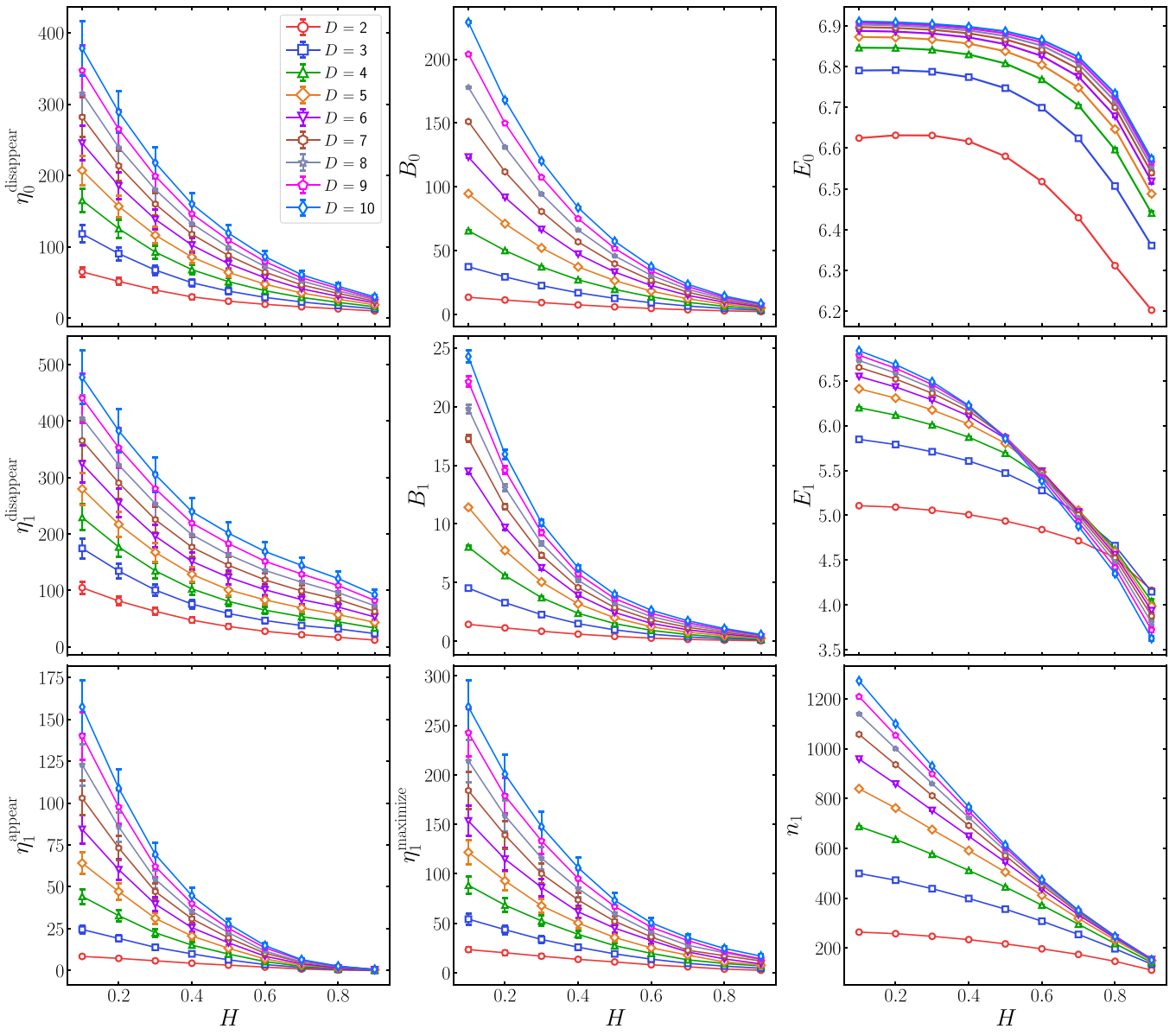

FIG. 7. The D dependency of topological measures introduced in this paper. We set the parameters as $\tau = 1$ and $q = 0$.

points in the unit D-cube (diameter). All proposed topological measurements in this work are computed and averaged over 10^3 realizations. For the computational part, we utilize the "Ripser" PYTHON package [74].

Now we are going to evaluate topological measures for the reconstructed phase space (embedded PCD) from generated fBm. We are interested in examining the effect of relevant parameters, namely, (H, q) (so-called intrinsic parameters) and (D, τ) (algorithmic parameters) on the dth homology group $(d = 0, 1)$. The upper panels of Fig. 5 show the dth PD ($d = 0$ filled blue diamond and $d = 1$ empty orange square) for Hurst exponents $H = 0.2, 0.5, 0.8$ (from left to right) for fixed parameters $D = 2$, $\tau = 100$, and $q = 0$. The insets are the visualization of the reconstructed PCD. The dth Betti curves of various H are also shown in the upper panels of Fig. 6. In this part, the parameters are $D = 4$, $\tau = 1$, and $q = 0$. These plots reveal how the topological distribution of state vectors in the D-cube and consequently the corresponding PDs and Betti curves change for various values of the Hurst exponent of the fBm series. The amount of memory encoded in the correlation quantity of the fBm signal impacts the pattern of reconstructed PCD, such that the higher value of H corresponding to a higher value of correlation in fBm leads to the continuous trajectory (slow changes) than does the lower value of correlation. In fact, by decreasing H, the N state vectors become randomly distributed in the D-cube. Almost all the proposed topological measures decrease by increasing the Hurst exponent for the various value of parameters D, τ, and q.

A. D dependency

The statistics and evolution of homology classes of PCD are strongly dependent on the dimension of the Euclidean

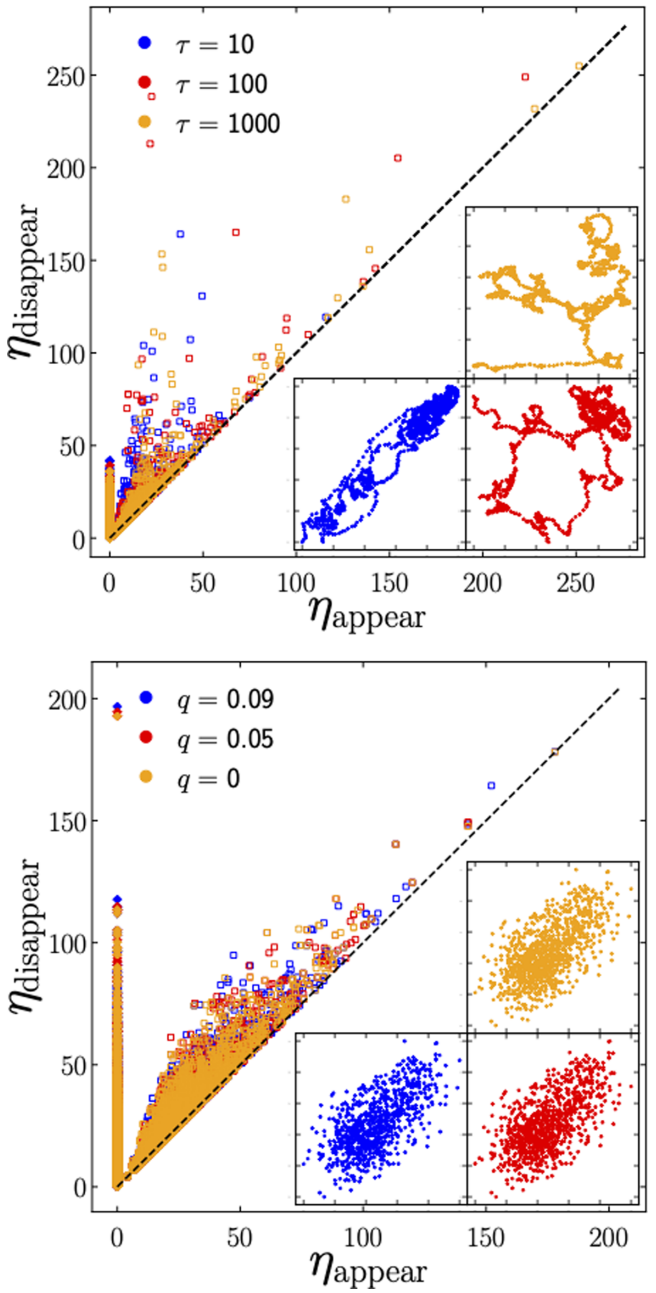

FIG. 8. Upper panel: The two-dimensional PCD of regular fBm with $H = 0.9$ for time delay $\tau = 10$ (blue), $\tau = 100$ (red), and $\tau = 1000$ (orange) and associated PDs (inset plots). Lower panel: the PDs of two-dimensional PCDs (insets) for $q = 0$ (orange), $q = 0.05$ (red), and $q = 0.09$ (blue); $H = 0.1$. In these plots, the associated zeroth and first PDs are represented by filled blue diamond and empty orange square symbols, respectively.

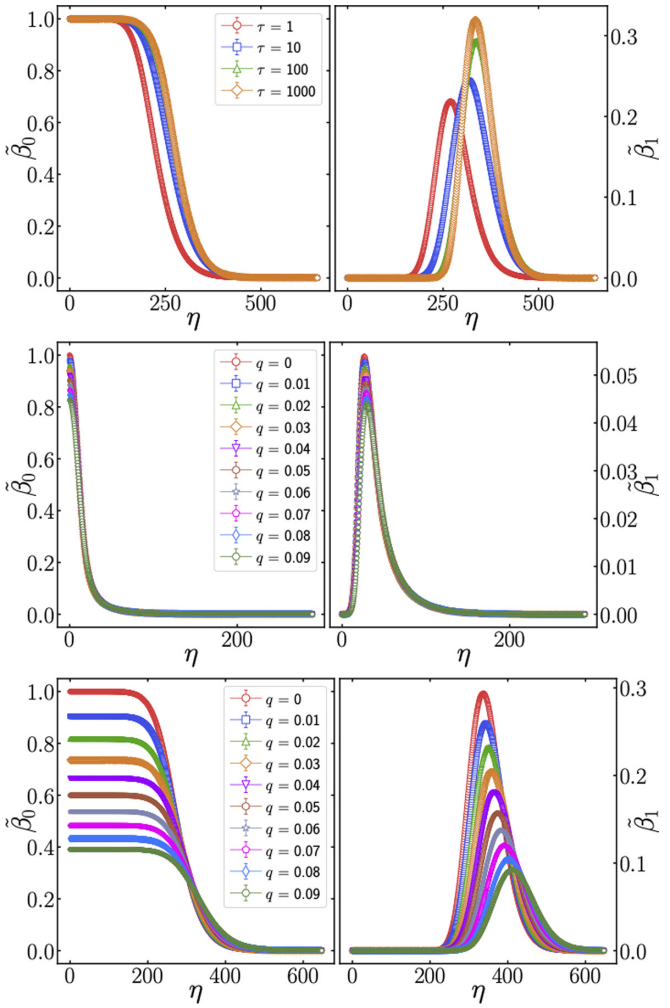

FIG. 9. Upper panels: The evolution of zeroth (left) and first (right) Betti number of reconstructed 10-dimensional phase space from regular fBm of $H = 0.1$ for different time-delay parameters. Middle panels: The number of connected components (left) and topological loops (right) for $D = 2$ and $H = 0.1$ as a function of threshold for various value of irregularity q. The lower panel is the same as the middle panel except for $D = 10$.

space as the embedding dimension. The zeroth (filled blue diamond) and first (empty orange square) PD of a regular ($q = 0$) embedded fBm with $H = 0.5$ by time delay $\tau = 1000$ to the 2-, 3-, and 4-cube is shown in the lower panels of Fig. 5. The inset plots are the projections of the reconstructed PCD into the standard two-dimensional planes $P_{ij} \equiv \{c_i\hat{e}_i + c_j\hat{e}_j \mid c_i, c_j \in \mathbb{R}\}$, where $\{\hat{e}_i\}_{i=1}^{D}$ is the standard basis of the space. The Betti curves for $d = 0$ and $d = 1$ of various D are also shown in the lower panels of Fig. 6. Since the typical distance between state vectors increases by increasing the embedding dimension for any given value of the Hurst exponent, the homology groups evolve (appeared, disappeared, and maximized) in the higher value of threshold (see also the lower panels of Fig. 5 as a consistent representation). The H dependency of the measures increases by D as shown in Fig. 7. This means that the topological differences between the distribution of state vectors for various H are more significant in higher dimensions, which can be captured by the homology classes. However, the sensitivity of E_0 for the fBm signal with $H \lesssim 0.5$ is less than other defined measures irrespective of the embedding dimension.

The interesting thing about the D dependency of the pattern of state vectors is that the topological distribution of these vectors for signals with $H \gtrsim 0.5$ is more robust versus the embedding dimension D. It is worth noting that the D dependency of the homology groups evolution is considerable when

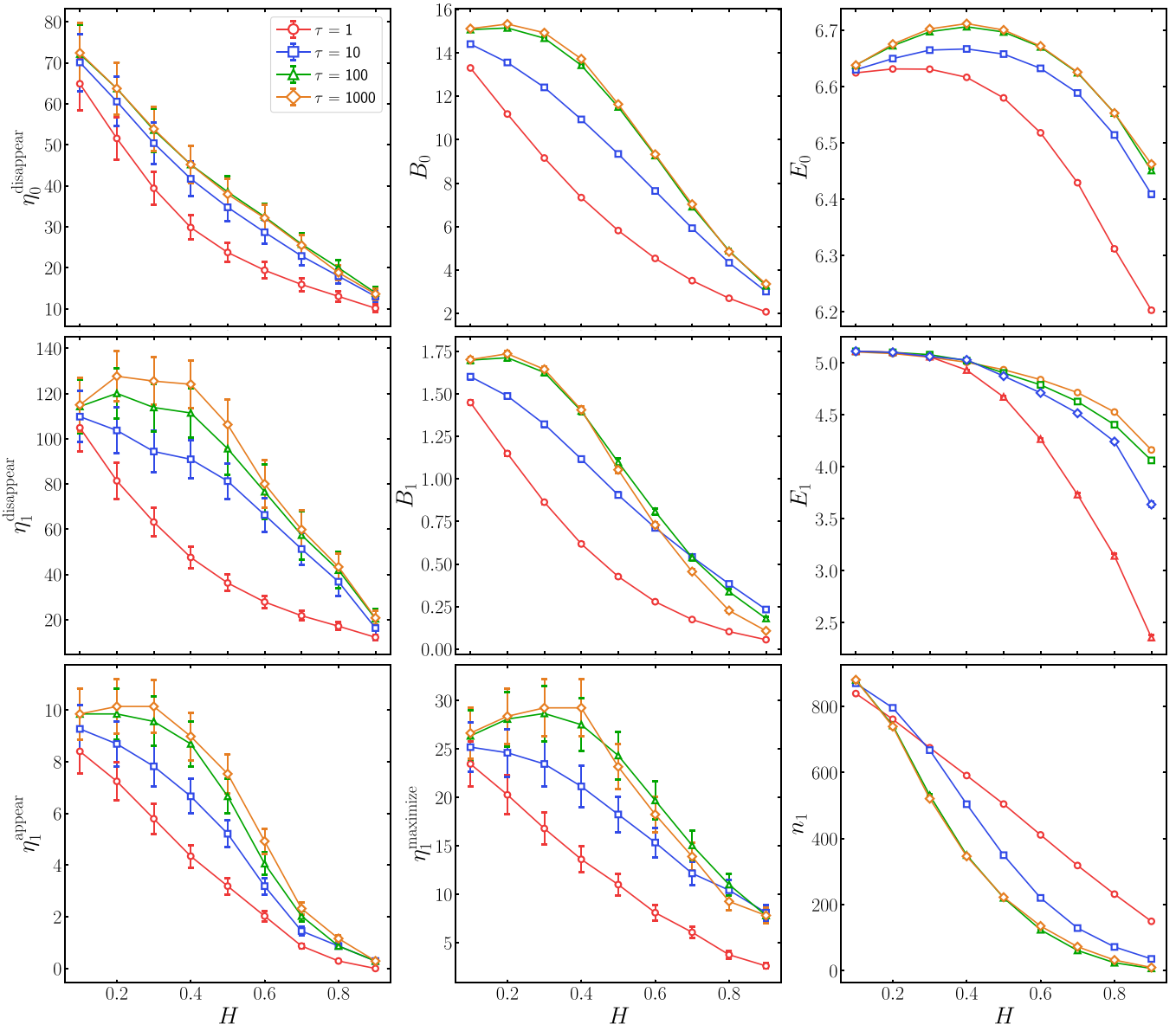

FIG. 10. The time-delay parameter τ impact on the H dependency of topological measures.

the embedded time series is irregular (we will discuss this in Sec. III C).

B. τ dependency

We consider a special case $\tau = 0$ for which the embedded PCD, $X(x, D, \tau = 0) = \{\vec{x}_t = (x_t, \ldots, x_t)\}_{t=1}^{L}$, is a subset of a line along $\vec{e} \equiv \sum_{i=1}^{D} \hat{e}_i$ with trivial topology, $\tilde{\beta}_d(H, q, N, D, \tau = 0, \eta) = 0$, $d > 0$, where $\{\hat{e}_i\}_{i=1}^{D}$ is the standard basis of D-dimensional Euclidean space. The upper panel of Fig. 8 illustrates a two-dimensional PCD reconstructed from highly correlated ($H = 0.9$) fBm for various time-delay values $\tau = 10, 100, 1000$, blue, red, and orange, respectively (inset plots) and associated PDs (filled diamond for $d = 0$ and empty square for $d = 1$). The higher value of τ leads to constructing a more extended PCD as shown in the insets plots of the upper panel of Fig. 8 and consequently the number of loops on the higher thresholds grows.

The Betti curves of a 10-dimensional PCD of fBm with $H = 0.1$ for various value of τ also are shown in the upper panel of Fig. 9. Figure 10 reveals the behavior of our proposed topological measures as a function of the Hurst exponent for various values of τ. Since the rate of the autocorrelation function decaying for the fBm time series decreases by increasing H, this suggests the small values of τ are more proper for estimating the Hurst exponent of the fBm series especially for the $H \lesssim 0.5$ regime, which is consistent with the statement in [67] from the network analysis point of view. For the almost $H \lesssim 0.5$ regime, the autocorrelation of the fBm signal goes down rapidly compared to that for $H \gtrsim 0.5$, and therefore as represented in different panels of Fig. 10, we find that for small τ our measures are sensitive as enough to estimate the Hurst exponent for the whole range

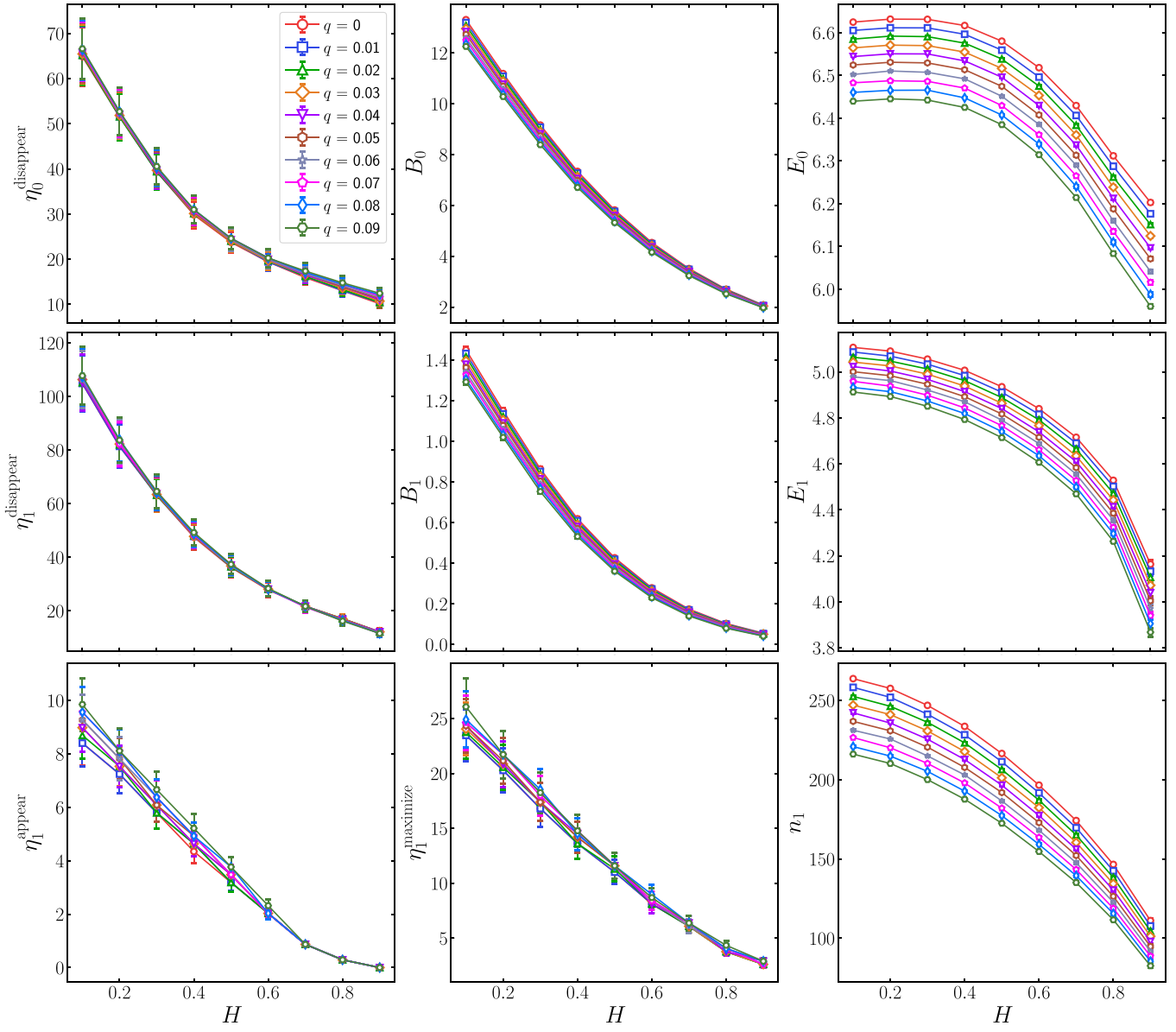

FIG. 11. The proposed measures as a function of the Hurst exponent for various amounts of irregularity controlled by q.

$H \in (0, 1)$ of the underlying fBm signal. In addition, our results demonstrate that particularly the E_0, E_1 and n_1 for large enough τ and small value of the Hurst exponent loose their H dependency.

C. q dependency

The lower panel of Fig. 8 shows the zeroth (filled diamond) and first (empty square) PD of two-dimensional PCDs (inset plots) converted from irregular ($q = 0$ orange, $q = 0.05$ red, and $q = 0.09$ blue) fBms with $H = 0.1$ by $\tau = 10$. The zeroth (middle left panel) and first (middle right panel) Betti curve of two-dimensional PCDs mapped from the fBm signal with $H = 0.1$ imposed by various irregularity q are illustrated in Fig. 9. The lower panels of Fig. 9 are for 10-dimensional PCDs, and the other parameters are the same as that for middle panels. This plot reveals the robustness of topological measures when we consider low-dimensional PCDs against the irregularity in the time series. To explain this fact, imposing irregularity on the time series x of length T makes the time series and embedded PCD X lose $T_{\text{missing}}(q) = qT$ data points and $N_{\text{missing}}(D, q) \geqslant T_{\text{missing}}$ state vectors, respectively. The number of missing state vectors N_{missing} strongly depends on the embedding dimension, such that $N_{\text{missing}}(D = 1, q) = T_{\text{missing}}$ and N_{missing} increases by D. To be precise, for a given irregular time series with irregularity equates to q, the number of missing data points in the series is $T_{\text{missing}} = qT$, and according to $N = T - (D - 1)\tau$, the influence of missing data points in the time series grows for higher values of D in state vectors of X. This effect can be recognized in the zeroth Betti number of X (see the beginning of the zeroth Betti curve in the middle and lower left panels of Fig. 9) as $N\tilde{\beta}_0(\eta = 0) = N(q) \leqslant T - (D - 1)\tau$. This phenomenon affects the behavior of topological measurements versus the Hurst exponent such

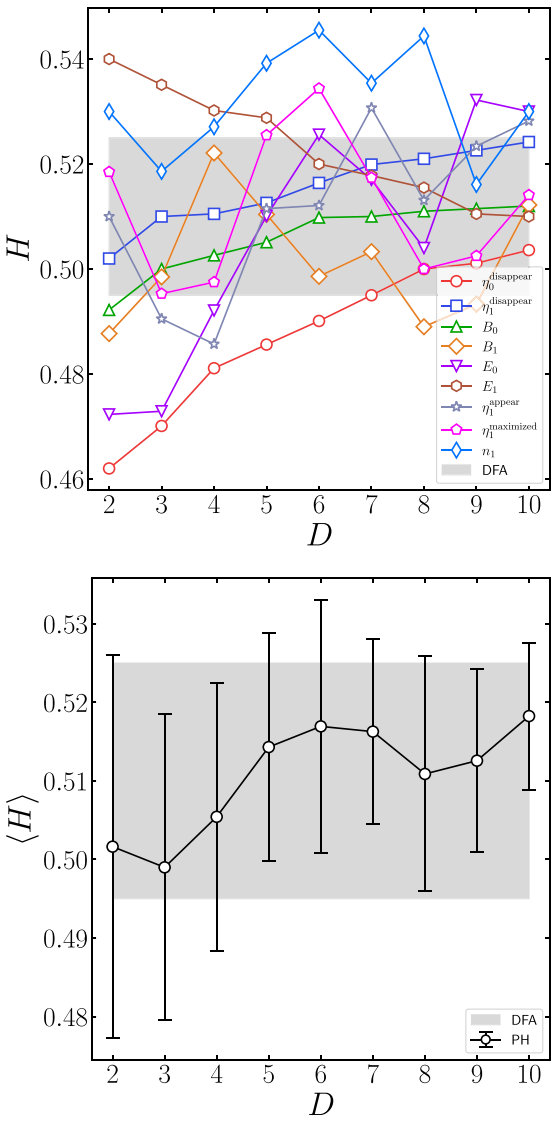

FIG. 12. Application of the proposed pipeline to S&P500 time series and corresponding Hurst exponent (upper panel) for computed topological measures as a function of embedding dimension D for fixed value of time delay $\tau = 1$. Lower panel illustrates the averaged Hurst exponent over topological measures and associated statistical error in the 1σ confidence interval as a function of D. The result based on the DFA method is shown by the gray area $H_{\text{DFA}} = 0.511 \pm 0.015$.

that some measures increase by q but some others decrease. This effect dramatically is high in higher dimensions (see Fig. 11).

IV. APPLICATION TO REALISTIC DATA

In order to show the capability of our proposed pipeline to characterize the self-similar nature of real data and to estimate the associated Hurst exponent, in this section we apply our approach to the financial time series of close prices in the Standard and Poor's 500 (S&P500) recorded daily from January 4, 2016, to December 31, 2019. The results are shown in Fig. 12. The upper panel of this figure indicates the value of the Hurst exponent as a function of the embedding dimension for the fixed time delay, $\tau = 1$, computed by our topological measures. D dependency of the mean value and statistical error at a 1σ confidence interval over the topological measures is illustrated in the lower panel of Fig. 12. Comparing our results to the Hurst exponent value based on the DFA method (the gray area in the upper and lower panels), which is $H_{\text{DFA}} = 0.511 \pm 0.015$, reveals the good consistency of the proposed method.

V. SUMMARY AND CONCLUDING REMARKS

In this work we studied the topological signatures based on the homology groups of a point cloud data (PCD) constructed from the synthetic fractional Brownian motion (fBm) series to classify these series using the corresponding Hurst exponent. We simulated the mock fBms for different H and converted them to a D-dimensional PCD (a discrete subset of the unit D-cube) according to the time-delay embedding (TDE) method for various embedding dimensions and time delays. Then by using the Vietoris-Rips (VR) method the embedded PCD is mapped into the simplicial complex for continuously varying proximity parameter ϵ and filtered by the persistent homology (PH) technique to capture the evolution of homology groups of triangulated PCD through the scales. For the zeroth and first homology group the homology classes are stored as pairs, so-called persistence pairs (PPs), in the zeroth and first persistence diagram (PD). Any PP contains an appearing and a disappearing scale for a homology class.

Relying on the population and distribution of PPs we defined the number of PPs and persistent entropy revealing the global properties of the corresponding PCD. Also, the zeroth and first Betti curves, $\beta_d(\epsilon)$, were computed to determine some transition scales for connectivity and loop structures in PCD. As we expected, all topological measures depend on the parameters $(H, q, D, \tau, \epsilon)$ shown in our pipeline (Sec. II C).

We assessed the H dependency of topological measures considered in this paper. Our results demonstrated that the H dependency of our measures ($\eta_0^{\text{disappear}}, B_0, E_0$ for the zeroth homology group, $\eta_1^{\text{appear}}, \eta_1^{\text{disappear}}, \eta_1^{\text{maximize}}, B_1, E_1, n_1$ for the first homology group) grows by increasing the embedding dimension (Fig. 7). The D dependency goes down for the higher value of the Hurst exponent since for this range of H, the amount of autocorrelation becomes high for a small time delay. The time-delay imprint on the topological measures has been illustrated in Fig. 10 demonstrating that the small value of τ is more reliable for determining the corresponding Hurst exponent in the whole range $H \in (0, 1)$ of synthetic fBm.

Motivated by irregularity existing in the realistic dataset in the universality class of fBm or fGn [33,59], an irregular mock series was simulated and quantified by a single irregular quantity (q). For the higher value of H, we expected the statistical properties of irregular fBm series remain almost unchanged. Our analysis showed that almost all topological criteria have weak dependency on q, and meanwhile E_0, E_1, and n_1 depended on irregularity existing in data (Fig. 11). This means that those measures which are more related to the size and ordering of data are more sensitive to q, and, consequently, we propose that taking into account $\eta_0^{\text{disappear}}$

and $\eta_1^{\text{disappear}}$ are more robust concerning data loss. In addition, the q dependency increases by increasing the embedding dimension. Also, we find that selecting the lower value of time delay makes a proper measure to estimate the value of the Hurst exponent for various types of fBm irrespective of irregularity.

For regular fBm series, the higher value of D, the more sensitive the behavior of topological measures is, while the influence of irregularity would be magnified for the higher value of the embedding dimension yielding the more H dependency happens for lower D. Reconstruction of a typical fBm series from a homology group can be carried out as follows: for a given value of the nine-dimensional feature vector or even one of our measures, we should determine the corresponding Hurst exponent according to the results indicated in Figs. 7 and 10. Then by using the Holmgren-Riemann fractional integral for mentioned H, the associated fBm series is generated.

Our final remarks are as follows: the size dependency of our proposed measures for any given value of the Hurst exponent is important to examine. Incorporating the embedding approach enables us to evaluate the higher-dimensional topological holes, which are nontrivial hidden shapes in the underlying series, particularly in the absence of irregularity. Both these tasks will be left for our future research.

ACKNOWLEDGMENTS

The authors are very grateful to B. Askari for his constructive comments. A part of the numerical simulations were carried out on the computing cluster of Brock University.

[1] M. C. Vuran, Ö. B. Akan, and I. F. Akyildiz, Comput. Netw. **45**, 245 (2004).
[2] P. J. Diggle, Monogr. Stat. Appl. Probab. **107**, 1 (2006).
[3] M. A. Chaplain, M. Ganesh, and I. G. Graham, J. Math. Biol. **42**, 387 (2001).
[4] G. Strang, G. Strang, G. Strang, and G. Strang, *Introduction to Linear Algebra*, Vol. 3 (Wellesley-Cambridge Press, Wellesley, MA, 1993).
[5] J. Defranza and D. Gagliardi, *Introduction to Linear Algebra with Applications* (Waveland Press, 2015).
[6] E. T. Jaynes, Phys. Rev. **106**, 620 (1957).
[7] C. H. Goulden, *Methods of Statistical Analysis* (Wiley, 1939).
[8] J. Mandel, *The Statistical Analysis of Experimental Data* (Courier Corporation, 2012).
[9] R. Albert and A.-L. Barabási, Rev. Mod. Phys. **74**, 47 (2002).
[10] L. da F. Costa, F. A. Rodrigues, G. Travieso, and P. R. Villas Boas, Adv. Phys. **56**, 167 (2007).
[11] M. Barthélemy, Phys. Rep. **499**, 1 (2011).
[12] Z. Wu, G. Menichetti, C. Rahmede, and G. Bianconi, Sci. Rep. **5**, 10073 (2015).
[13] M. Boguñá, I. Bonamassa, M. De Domenico, S. Havlin, D. Krioukov, and M. Serrano, Nat. Rev. Phys. **3**, 114 (2021).
[14] R. J. Adler, *The Geometry of Random Fields*, Vol. 62 (SIAM, 1981).
[15] G. Carlsson, Bull. Am. Math. Soc. **46**, 255 (2009).
[16] S. O. Rice, Bell Labs Tech. J. **23**, 282 (1944).
[17] S. O. Rice, Bell Syst. Tech. J. **24**, 46 (1945).
[18] S. Rice, *Mathematical Analysis of Noise, Noise and Stochastic Processes*, edited by N. Wax (Dover Publications, New York, 1954).
[19] J. M. Bardeen, J. R. Bond, N. Kaiser, and A. S. Szalay, Astrophys. J. **304**, 15 (1986).
[20] T. Matsubara, Astrophys. J. **584**, 1 (2003).
[21] D. Pogosyan, C. Pichon, C. Gay, S. Prunet, J. Cardoso, T. Sousbie, and S. Colombi, Mon. Not. R. Astron. Soc. **396**, 635 (2009).
[22] C. Gay, C. Pichon, and D. Pogosyan, Phys. Rev. D **85**, 023011 (2012).
[23] T. Matsubara and S. Codis, Phys. Rev. D **101**, 063504 (2020).
[24] A. Vafaei Sadr and S. Movahed, Mon. Not. R. Astron. Soc. **503**, 815 (2021).
[25] B. Mandelbrot, *The Fractal Geometry of Nature* (W. H. Freeman, San Francisco, 1982).
[26] A typical $(N + D)$-dimensional stochastic field (process) is a measurable mapping from probability space into a $\mathbb{R}^N$-valued function on an $\mathbb{R}^D$ Euclidean space, in which the labels N and D are, respectively, assigned to N-dependent and D-independent parameters, generating a $(N + D)$-dimensional random field or a stochastic process.
[27] H. E. Hurst, Trans. Am. Soc. Civ. Eng. **116**, 770 (1951).
[28] B. B. Mandelbrot and J. W. Van Ness, SIAM Rev. **10**, 422 (1968).
[29] C.-K. Peng, S. V. Buldyrev, S. Havlin, M. Simons, H. E. Stanley, and A. L. Goldberger, Phys. Rev. E **49**, 1685 (1994).
[30] C.-K. Peng, S. Havlin, H. E. Stanley, and A. L. Goldberger, Chaos **5**, 82 (1995).
[31] J. W. Kantelhardt, S. A. Zschiegner, E. Koscielny-Bunde, S. Havlin, A. Bunde, and H. E. Stanley, Physica A **316**, 87 (2002).
[32] Z.-Q. Jiang, W.-J. Xie, W.-X. Zhou, and D. Sornette, Rep. Prog. Phys. **82**, 125901 (2019).
[33] I. Eghdami, H. Panahi, and S. Movahed, Astrophys. J. **864**, 162 (2018).
[34] T. K. Dey and Y. Wang, *Computational Topology for Data Analysis* (Cambridge University Press, 2022).
[35] H. Edelsbrunner and J. L. Harer, *Computational Topology: An Introduction* (American Mathematical Society, 2022).
[36] A. J. Zomorodian, *Topology for Computing*, vol. 16 (Cambridge University Press, 2005).
[37] R. Ghrist, Bull. Am. Math. Soc. **45**, 61 (2008).
[38] L. Wasserman, Annu. Rev. Stat. Appl. **5**, 501 (2018).
[39] M. Nakahara, *Geometry, Topology and Physics* (CRC Press, 2003).
[40] J. R. Munkres, *Elements of Algebraic Topology* (CRC Press, 2018).
[41] A. Hatcher, *Algebraic Topology* (Tsinghua University Press Co., Ltd., 2005).
[42] N. Otter, M. A. Porter, U. Tillmann, P. Grindrod, and H. A. Harrington, EPJ Data Sci. **6**, 17 (2017).
[43] L. Speidel, H. A. Harrington, S. J. Chapman, and M. A. Porter, Phys. Rev. E **98**, 012318 (2018).

[44] S. Maletić, Y. Zhao, and M. Rajković, Chaos **26**, 053105 (2016).
[45] I. Donato, M. Gori, M. Pettini, G. Petri, S. De Nigris, R. Franzosi, and F. Vaccarino, Phys. Rev. E **93**, 052138 (2016).
[46] C. M. Pereira and R. F. de Mello, Expert Syst. Appl. **42**, 6026 (2015).
[47] H. Masoomy, B. Askari, S. Tajik, A. K. Rizi, and G. R. Jafari, Sci. Rep. **11**, 16414 (2021).
[48] L. Lacasa, B. Luque, F. Ballesteros, J. Luque, and J. C. Nuno, Proc. Natl. Acad. Sci. USA **105**, 4972 (2008).
[49] Y. Yang and H. Yang, Physica A **387**, 1381 (2008).
[50] F. Takens, in *Dynamical Systems and Turbulence, Warwick 1980* (Springer, 1981), pp. 366–381.
[51] N. H. Packard, J. P. Crutchfield, J. D. Farmer, and R. S. Shaw, Phys. Rev. Lett. **45**, 712 (1980).
[52] Z. Gao and N. Jin, Phys. Rev. E **79**, 066303 (2009).
[53] N. Marwan, J. F. Donges, Y. Zou, R. V. Donner, and J. Kurths, Phys. Lett. A **373**, 4246 (2009).
[54] R. V. Donner, Y. Zou, J. F. Donges, N. Marwan, and J. Kurths, New J. Phys. **12**, 033025 (2010).
[55] Y. Shimada, T. Kimura, and T. Ikeguchi, in *International Conference on Artificial Neural Networks* (Springer, 2008), pp. 61–70.
[56] K. Hu, P. C. Ivanov, Z. Chen, P. Carpena, and H. E. Stanley, Phys. Rev. E **64**, 011114 (2001).
[57] Z. Chen, P. C. Ivanov, K. Hu, and H. E. Stanley, Phys. Rev. E **65**, 041107 (2002).
[58] R. Nagarajan and R. G. Kavasseri, Physica A **354**, 182 (2005).
[59] Q. D. Y. Ma, R. P. Bartsch, P. Bernaola-Galván, M. Yoneyama, and P. C. Ivanov, Phys. Rev. E **81**, 031101 (2010).
[60] L. Lacasa, B. Luque, J. Luque, and J. C. Nuno, Europhys. Lett. **86**, 30001 (2009).
[61] X.-H. Ni, Z.-Q. Jiang, and W.-X. Zhou, Phys. Lett. A **373**, 3822 (2009).
[62] W.-J. Xie and W.-X. Zhou, Physica A **390**, 3592 (2011).
[63] H. Masoomy and M. Najafi, arXiv:2112.07698 (2021).
[64] J.-L. Liu, Z.-G. Yu, and V. Anh, Phys. Rev. E **89**, 032814 (2014).
[65] M. B. Kennel, R. Brown, and H. D. I. Abarbanel, Phys. Rev. A **45**, 3403 (1992).
[66] A. M. Fraser and H. L. Swinney, Phys. Rev. A **33**, 1134 (1986).
[67] Y. Zou, R. V. Donner, and J. Kurths, Phys. Rev. E **91**, 022926 (2015).
[68] H. Masoomy, B. Askari, M. N. Najafi, and S. M. S. Movahed, Phys. Rev. E **104**, 034116 (2021).
[69] A. Myers, E. Munch, and F. A. Khasawneh, Phys. Rev. E **100**, 022314 (2019).
[70] B. H. Arnold, *Intuitive Concepts in Elementary Topology* (Courier Corporation, 2011).
[71] E. Munch, J. Learn. Anal. **4**, 47 (2017).
[72] J.-P. Kahane, *Some Random Series of Functions*, Vol. 5 (Cambridge University Press, 1993).
[73] I. S. Reed, P. Lee, and T.-K. Truong, IEEE Trans. Inf. Theory **41**, 1439 (1995).
[74] C. Tralie, N. Saul, and R. Bar-On, J. Open Source Softw. **3**, 925 (2018).